HEAT DIFFUSION BASED DETECTION OF COLONIC POLYPS IN CT COLONOGRAPHY

[1]*Ender Konukoğlu,* [1]*Burak Acar,* [2]*David S. Paik,* [2]*Christopher F. Beaulieu, and* [2]*Sandy Napel*

[1]Boğaziçi University/Department of Electrical and Electronics Eng. İstanbul, Turkey
{konukoge,acarbu}@boun.edu.tr
[2]Stanford University/Department of Radiology, Stanford, CA, USA
{termite,rtemple,snapel}@stanford.edu

ABSTRACT

Computer Aided Detection (CAD) in Computed Tomography Colonography (CTC) aims at detecting colonic polyps that are the precursors of cancer. We propose a polyp detection / identification algorithm with a built-in enhancement scheme. The underlying idea of the proposed method is to utilize the nonlinear heat diffusion process, which is closely related to the nonlinear diffusion filtering, to generate a vector field that is correlated with the shape of the colon wall. The nonlinearity is used to specifically enhance the difference between polyp and nonpolyp structures to improve the detection and the identification performance. The method was evaluated on real patient CTC data acquired from a polyp-rich volunteer. 3 FPs (17 FPs) were achieved at 6/7 (7/7) sensitivity levels for polyps larger than 8mm.

1. INTRODUCTION

Computed Tomographic Colonography (CTC) is a minimally invasive technique that employs X-Ray CT imaging of the abdomen and pelvis following cleansing and air insufflation of the colon. Originally proposed in the early 1980's [1], it became practical in the early 1990's following the introduction of helical CT and advances in computer graphics. Currently available multi-slice helical X-Ray CT scanners are capable of producing hundreds of high resolution ($< 1mm$ cubic voxel) images in a single breath hold. Conventional examination of these source images is rather time-consuming and the detection accuracy is unavoidably limited by human factors such as attention span and eye fatigue. Several visualization and navigation techniques have already been proposed to help the radiologists [2–5]. However, computer aided detection (CAD) tools are envisioned to improve the efficiency and the accuracy beyond what can be achieved by visualization techniques alone [6–13]. Several studies have investigated CAD for CTC. Vining et al. used abnormal colon wall thickness to detect colonic polyps [6]. Summers et al. used the mean, the gaussian and the principal curvatures of the colon surface and showed good preliminary results for phantom and patient data [7, 8]. Kiss et al. used surface normals along with sphere fitting [9], while Yoshida et al. used both the pre-segmented surface differential characteristics captured by a shape index, and the gradient vector field of the CT data [10]. The proposed surface normal overlap (SNO) algorithm is based on the observation that for locally spherical and hemispherical structures, large numbers of surface normals intersect near the centers of these structures [11]. To improve specificity, Göktürk et al. used triples of randomly oriented orthogonal cross-sectional images of pre-detected suspicious structures which are then classified by support vector machines [12], while Acar et al. modeled the way radiologists utilize 3D information as they are examining a stack of 2D images as an Edge Displacement Field (EDF) [13]. We propose the Heat Diffusion Field (HDF) method as a way to detect and characterize polyps represented as a surface in 3D. The HDF method is a 3D detection and characterization method built on the well-known nonlinear diffusion filtering framework. This has the effect of *forcing* the diffusion to form a diffusion pattern singularity near the centers of protruding structures, like polyps. This enhancing property is the main advantage of HDF over previously proposed methods, like EDF, SNO and the Gradient Concentration [10] and, to the best of our knowledge, is the first enhancing scheme proposed for CTC. The HDF method is based on detecting and characterizing those sinks thus generated in conjunction with local voxel distribution around them. The method was evaluated using CT data from a single harboring 7 polyps with diameters $\geq 8mm$. The paper is organized as follows: We explain the algorithm in Section 2. Section 3 explains the evaluation methodology. Section 4 discusses the results based on real patient data experiments. In Section 5, we further discuss our algorithm and the results. The concluding remarks are given in Section 6.

This work was in part supported by TUBITAK (National Science Foundation of Turkey) as a part of the KARIYER-DRESS project, and in part supported by NIH (National Institute of Health) under grant NIH R01-CA72023.

2. THE HDF ALGORITHM

The primary observation is that if the colon lumen is thought to be initially heated to a constant level, then the heat diffusion process would generate local heat diffusion pattern singularities (sinks) near the centers of protruding structures. This can further be enhanced by using a nonlinear diffusion scheme that depends on the curvature of iso-temperature surfaces of the diffusing heat field, where initially the colon wall itself is the only isotemperature surface. The diffusion proceeds faster in regions where the isotemperature surfaces are concave (necks of protruding structures) rather than convex (apex of protruding structures). In other words, nonlinear diffusion schemes effect is to have higher diffusion coefficients at the bases of protruding structures with respect to their apex. The diffusion pattern can be described by a vector field $\mathbf{V}(\mathbf{r}), \mathbf{r} = [x\ y\ z]^T$ that is generated by tracking the motion of the isotemperature surfaces along their normal directions. $\mathbf{V}$ would have the aforementioned singularities near the centers of such structures. It is thus used to detect suspicious locations. Both the vector field geometry and local voxel distribution around such detected points are used to identify the polyps.

2.1 Segmentation

First, the colon lumen in each subvolume is segmented by simple thresholding followed by morphological filtering as follows: The CT data are converted to a binary volume ($S(\mathbf{r})$) by thresholding at 350 HU ($CT(\mathbf{r}) > 350HU \Rightarrow S(\mathbf{r}) = 1 \quad o.w. \quad S(\mathbf{r}) = 0$). $S(\mathbf{r}) = 0$ are the air voxels. Next, the isolated 1's in $S(\mathbf{r})$ are removed and 26-neighborhood morphological closing followed by a thinning operation is performed on the binary volume S to filter out segmentation noise using *Matlab*'s built-in functions. Thus $S = 1$ represents the tissue while its complement represents the colon lumen.

2.2 The HDF Computation

The algorithm starts with the segmented colon lumen, $\{\mathbf{r}|S(\mathbf{r})=0\}$, set to a constant temperature, $T_0 = 1$. It is then allowed to cool. The diffusion process in governed by the nonlinear PDE given in Equation 1 [14]. $T(\mathbf{r},t)$ stands for the temperature at position $\mathbf{r}$ at time t. Equation 1 relates the rate of change in $T(\mathbf{r},t)$ throughout the domain, to the divergence of the gradient of $T(\mathbf{r},t)$ weighted by some scalar weight. The weighting factor, given by g, is the isotropic diffusion coefficient. Equation 2 relates this change in temperature to an instantaneous vector field $\mathbf{v}(\mathbf{r},t)$ that represents the motion of the iso-temperature surface along its normal direction at the given position and time.

$$\frac{\partial T(\mathbf{r},t)}{\partial t} = \nabla \cdot g(\kappa(\mathbf{r},\mathbf{t}),t)\nabla T(\mathbf{r},t) \quad (1)$$

$$\frac{\partial T(\mathbf{r},t)}{\partial t} = -\nabla T(\mathbf{r},t)\cdot \mathbf{v}(\mathbf{r},t) \quad (2)$$

where

$$g(\kappa,t) = \begin{cases} \frac{-5\,arctan(1.2\kappa)+\frac{5\pi}{2}+0.1}{5\pi+0.1} \times D_{max} & t \le N\Delta t \\ D_{max} & t > N\Delta t \end{cases} \quad (3)$$

where $\kappa = \kappa(\mathbf{r},t)$ is the mean curvature of the iso-temperature surface passing through the point $\mathbf{r}$ at time t calculated from $T(\mathbf{r},t)$, which is an implicit function for all iso-temperature surfaces [15]. This nonlinear function is not necessarily the only function that can be used, other monotically decreasing functions of κ with smooth transition are expected to perform similarly. $\Delta t = 0.1$ is the discretization time step. D_{max} is the upper bound for the diffusion coefficient (emprically set as 5). Equation 3 states that a nonlinear spatially varying diffusion coefficient is applied during the first N iterations (empirically set as 5). The rest of the diffusion process is linear isotropic diffusion with a diffusion coefficient of D_{max}. The role of g is to increase diffusion in regions with concave ($\kappa < 0$) iso-temperature surfaces (like the base of polyps) with respect to the convex ($\kappa > 0$) regions (like the apex of polyps)
Equating Equations 1 and 2, we get,

$$\begin{aligned} -\nabla \cdot g\nabla T(\mathbf{r},t) &= \nabla T(\mathbf{r},t)\cdot \mathbf{v}(\mathbf{r},t) \\ T(\mathbf{r}\in\{S(\mathbf{r})=0\},t=0) &= T_0 \end{aligned} \quad (4)$$

where g represents the nonlinear diffusion coefficient as given above. We can define the vector field $\mathbf{V}(\mathbf{r})$ as

$$\begin{aligned} \mathbf{V}(\mathbf{r}) &= \int_0^{\tau} |\nabla T(\mathbf{r},t)|\mathbf{v}(\mathbf{r},t)\,dt\,, \qquad \mathbf{v} \parallel \nabla T \\ &= \int_0^{\tau} \left(\frac{\nabla T(\mathbf{r},t)}{|\nabla T(\mathbf{r},t)|}\right)\left(-\nabla \cdot g\nabla T(\mathbf{r},t)\right) dt \\ &\quad , T(\mathbf{r},t) < 0.1 \end{aligned} \quad (5)$$

The HDF is the resultant vector field $\mathbf{V}(\mathbf{r})$ that is the integral of instantaneous field $\mathbf{v}(\mathbf{r},t)$ weighted by the temperature gradient over time (Equation 5) in regions where the current temperature is less than 0.1. $T(\mathbf{r},t) < 0.1$ makes sure that mainly the leading heat front contributes to $\mathbf{V}(\mathbf{r})$. The geometrical characteristics of $\mathbf{V}$ will be used during the detection and the identification of colonic polyps together with a second parameter TU (Sections 2.3 and 2.4).

Numerical computation of the HDF, $\mathbf{V}(\mathbf{r})$, is done using Equation 5, where the continuous integration is replaced by discrete summation over a finite number of time intervals. The isotropic diffusion term in Equation 5 is solved numerically using the *Alternating-Direction Implicit (ADI) Method*, which is said to guarantee numerical stability [**?**]. The numerical differentiation was done using a Gaussian derivative kernel with $\sigma = 0.6mm$ and $\pm 2\sigma$ kernel support. Figure 1 shows the heat distribution at different stages of the diffusion in the vicinity of a 8.9 mm polyp. The heat diffusion pattern singularity around the polyp center is apparent.

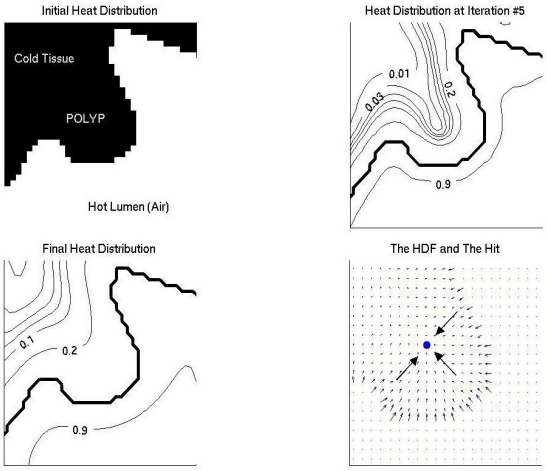

Figure 1: Isotemperature contour plots on the central slice across a 8.9 mm polyp (Clockwise from top left figure) a) just before diffusion starts, b) at the end of the nonlinear diffusion part, c) after the final iteration (The bold line marks the colon wall), d) computed vector field with the detected HDF hit marked, yielding a FA value of 0.028 (the figure is zoomed for visual purposes).

2.3 Detection

The proposed nonlinearity of the diffusion process is aimed at generating spherically symmetric singularities in the vicinity of polyp centers. A perfectly spherically symmetric vector field is not achievable due to polyp shape variations; however, it can be approached. The differential characteristics of $\mathbf{V}$ are summarized by its Jacobian matrix $\mathbf{J}$. For $\mathbf{V}(\mathbf{r})$ (a 3D vector field), $\mathbf{J}$ is defined as follows:

$$\mathbf{J} = \begin{bmatrix} \frac{\partial V_x}{\partial x} & \frac{\partial V_x}{\partial y} & \frac{\partial V_x}{\partial z} \\ \frac{\partial V_y}{\partial x} & \frac{\partial V_y}{\partial y} & \frac{\partial V_y}{\partial z} \\ \frac{\partial V_z}{\partial x} & \frac{\partial V_z}{\partial y} & \frac{\partial V_z}{\partial z} \end{bmatrix} \quad (6)$$

The sinks sought correspond to the vector field points where the eigenvalues (λ's) of $\mathbf{J}$ have all negative real parts close to each other. Their closeness (i.e. the spherical symmetry of $\mathbf{V}(\mathbf{r})$) can be measured using the *Fractional Anisotropy* parameter which is defined as,

$$FA = \sqrt{\frac{3}{2}}\sqrt{\frac{(\alpha_1-\overline{\alpha})^2+(\alpha_2-\overline{\alpha})^2+(\alpha_3-\overline{\alpha})^2}{(\alpha_1^2+\alpha_2^2+\alpha_3^2)}} \quad (7)$$

where $\alpha_i = Real(\lambda_i)$, $i = \{1,2,3\}$ and $\overline{\alpha}$ is the mean of α's. *FA* represents the geometrical information embedded in the HDF. *FA* is between 0 and 1, and $FA = 0$ for perfectly spherically symmetric singularities, hence the smaller the *FA* is, the more probable the structure is a polyp, provided that $\alpha_i < 0, \quad i = 1,2,3$. The 3D Watershed Transform is used to segment the 3D buckets (watershed basins in 3D) in the 3D FA map (i.e. the geometry map, $FA(x,y,z)$, in $\Re^3$) generated as explained above. The minimum FA point in each bucket is marked as a "hit"(i.e., a polyp candidate). This stage is summarized in Figure 2.

2.4 Identification

The *FA* parameter quantifies the spherical symmetry and is especially useful in discriminating folds from polyps. The elongated structure of the folds results in a $\mathbf{V}(\mathbf{r})$ that is 2D symmetric *only* on the plane perpendicular to the fold's main axis. This means $min_i\{|\alpha_i|\} \cong 0$ which results in high *FA* values. However, *FA* alone

1. *Compute* $\alpha_i = Real(\lambda_i)$, $i = \{1,2,3\}$ *for the whole volume.*
2. *Mark all points with* $\alpha_i < 0$, $i = \{1,2,3\}$ *as Valid Points and compute the FA values for these points.*
3. *Assign* $FA = -\infty$ (a value required by $Matlab^{TM}$'s built in *watershed* function) *for all Non-Valid Points and segment the FA volume created in Step 3 using the watershed transform (WT). WT labels the FA buckets in 3D.*
4. *Exclude the FA buckets that touch the volume boundaries.*
5. *Mark the minimum FA points in each bucket as an HDF Hit as long as it is in the tissue.*

Figure 2: The HDF geometry based detection algorithm

is not sufficient to eliminate all non-polyp hits. There are hits with low *FA* values just because there are nearby air voxels distributed around somewhat uniformly, like at the junction of folds. To overcome this problem, we perform a local analysis of the colon wall around the hits and compute a *Triangle Area Uniformity (TU)* parameter. *TU* is used together with *FA* for identification.

The primary idea behind *TU* is that there should be air voxels around a polyp that are directionwise uniformly distributed over a spherical surface patch (colon wall). We mark the azimuth and the elevation angles of the closest air voxels within a certain distance (15mm is used as an arbitrary choice[1]) in M directions (M=100 as an arbitrary choice) on a unit sphere. These points should form a single cluster on the unit sphere for polyps and be uniformly distributed within this cluster. We perform a Delaunay Triangulation of the surface defined by these points and use the number of triangles and the trimmed variance of their areas to measure this as follows:

$$\begin{aligned} A_i \text{ , } i = 1,\cdots,K &: \text{Triangle areas} \\ \tilde{A} &= \{\text{Smaller 90\% of } A_i's\} \\ \sigma^2_{\tilde{A}} = VAR_i(\tilde{A}) \text{ , } TU &= \frac{\tilde{K}}{\sigma^2_{\tilde{A}}} \end{aligned} \tag{8}$$

where $\tilde{K}$ denotes the number of triangles in the reduced set $\tilde{A}$. The largest 10% of the A_i's are excluded from the variance calculation because the polyps are more likely to be hemispherical structures, hence the large triangles formed at the bases of polyps increase $\sigma^2_{\tilde{A}}$ artificially. *TU* is larger for polyps.

3. EVALUATION METHODOLOGY

We used Free Response Receiver Operator Characteristic (FROC) curves to evaluate the performance of our algorithm [16]. FROC curves show the trade-off between sensitivity (detection rate of true positives) and the detection rate of false positives. They are especially suitable for the performance evaluation of detection algorithms as opposed to pure classification algorithms as the set of negatives is not well-defined. In other words, all points in the 3D data except the inner regions of polyps are potential negatives. Since this corresponds to using a large number in the denominator for the conventional definition of specificity, it would be misleading.

We used CTC data acquired from a 56 year old female patient for evaluation. The patient was scanned in the prone position in an 8 slice multi-detector row CT scanner (GE Lightspeed Ultra, Milwaukee, WI) in the 4 slice helical mode (slice width=2.5mm, pitch=0.75, slice spacing=1.25mm, FOV=36cm reconstructed on a 512×512 matrix, kV=120, mA=120). She underwent fiberoptic colonoscopy immediately after the CT scan 47 polyps were reported by the radiologist - 7 larger than 8 mm. A thousand and two hundred fifty subvolumes of $30mm^3$ with $10mm$ overlap at every end, covering the whole colon wall were processed. The average voxel spacing was $0.74mm \times 0.74mm \times 1.31mm$ and the data were interpolated to $0.6mm \times 0.6mm \times 0.6mm$ prior to processing. A wide range of polyp shapes were present in the dataset.

The gold standard was generated by a radiologist with 8 years of experience in CTC, who marked the centers of FOC (Fiber Optic Colonoscopy) confirmed polyps and measured their diameters using a custom built computer program. Those center points and the diameter measurements specify spherical regions. All hits in such a sphere are considered as TPs associated with the same polyp and are labeled accordingly. Assuming that the vector fields around the detected sinks inside the true polyps are more spherically symmetric than sinks associated with nonpolyp structures, we sorted all of the detected points with respect to *FA* in a descending order. We then went through this list starting from the top, keeping the top most one and eliminating all of the other points that were, closer to that hit than the radius of the smallest polyp of interest (ξ), as set by the user. The underlying idea is that the centers of two polyps of interest (assumed to be a hemispherical structures in general) can not be closer to each other than ξ. We also limited ξ to be larger than or equal to $1.5mm$. This process also eliminates multiple hits which may occur due to using overlapping subvolumes. This grouping strategy is only based on the a priori preference that the user (the radiologist) would have made regarding the size of polyps he/she was interested in, simulating a clinical application. The final identification is done on the 2D (FA, TU) domain using simple thresholding. An *FA* threshold,ε_{FA}, and a *TU* threshold, ε_{TU}, are varied through the list of hits, Ω. The subset of Ω with $FA < \varepsilon_{FA}$ *AND* $TU > \varepsilon_{TU}$ is the output positive set, Ψ. If a point in Ψ is within a polyp (defined by the polyp center and diameter, as determined by the radiologist setting the gold standard) then it is associated with that polyp and labelled, otherwise it is left unlabelled. The number of points in Ψ that are left unlabelled is the number of FPs at that $(\varepsilon_{FA}, \varepsilon_{TU})$ pair. The number of TPs is the number of polyps with at least one voxel (from the inner region of that polyp) in Ψ. Multiple detections within a single polyp are considered as a single TP. A 1D FROC curve is computed for each ε_{FA}. The combination of these curves make up a 2D FROC surface. The evaluation is based on the FP and sensitivity rates corresponding to $(\varepsilon_{FA}, \varepsilon_{TU})$ pairs.

4. RESULTS

Only the clinically significant polyps ($\geq 8mm$) were considered, i.e., all hits associated with small polyps were excluded from the performance analysis. The *FA* parameter was used as a pre-detector in the following way. We computed 1D FROC curves by varying the *TU* parameter on the set of hits with $FA \leq \varepsilon_{FA}$, where ε_{FA} is the *FA* threshold. For $\varepsilon_{FA} = 0.2411$, the FROC curve resulted in 17 FPs at 7/7 sensitivity and 7 FPs at 6/7 sensitivity. For a lower ε_{FA} ($\varepsilon_{FA} = 0.1213$) we missed one of the 7 polyps but suffered 3 FPs at 6/7 sensitivity. The missed polyp was $10.4mm$ in diameter and was located at the junction of folds. Figure 3 summarizes the above results. The algorithm was implemented using $Matlab$6.5 and run on an $Intel^{TM}$ $Pentium^{TM}$4 based PC with 2.40 GHz clock speed and 1GB RAM. It took 10 seconds to process each $30mm^3$ subvolume ($51 \times 51 \times 51$ voxels).

5. DISCUSSION

The HDF has a built-in enhancement scheme due to the embedded nonlinearity and it has a geometrical analysis component that enables the HDF algorithm to discriminate polyps from elongated protruding structures like the haustral folds. Unlike a vector field that could have been generated using the SNO method or the distance transform, the HDF is designed to generate spherically more symmetric sinks in the case of sessile polyps. To the best of our knowledge, HDF is the first polyp enhancing scheme proposed.

The second stage of the algorithm considers the colon wall

[1]This limit is related to the radius of the maximum polyp size we are interested in.

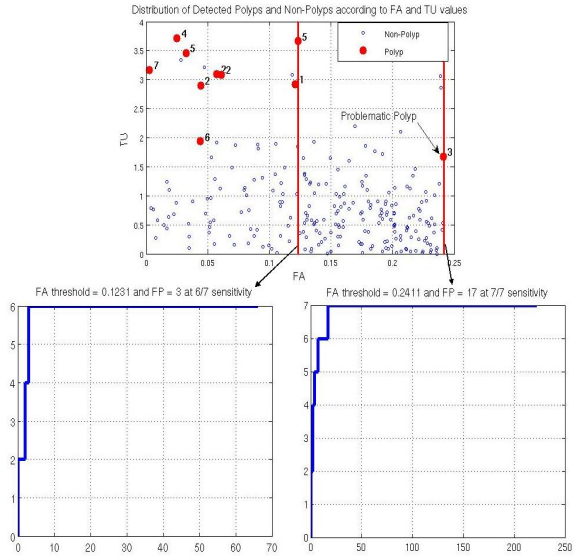

Figure 3: Top: The *FA* vs *TU* distribution of the HDF hits for polyps larger than 8mm in diameter.Bottom: Two FROC curves for two different *FA* thresholds.

topology around the detected point. The *TU* parameter does not deal with the colon wall characterization, as previously proposed methods do [10], but rather focuses on identifying non-protruding structures surrounded by air voxels, which may lead to vector field singularities with low FA values like junctions of folds. The *TU* parameter quantifies the clustering of these air voxels around the vector field singularity. Despite being a local parameter, it considers a subvolume large enough to enclose a polyp. As such, it is a global parameter for structures of the size of a polyp.

The method performed poorly on one of the 7 polyps that were larger than 8mm in diameter. This polyp had a diameter of 10.4mm and was situated at a junction of folds and, thus, had a higher FA value than other polyps of similar size.This resulted in the accrual of a large number of false positives.

The method uses simple thresholding in a 2D parameter space of *FA* and *TU*. A better scheme of identification would be to train a general purpose classifier to discriminate between polyps and non-polyps. However, significantly more data is required train and test such a classifier.

An evaluation on a larger dataset is required to assess the HDF method more thoroughly. A valuable assessment of any CTC CAD algorithm would be to measure the algorithm's performance in discriminating patients with polyps from the ones without any polyps.

6. CONCLUSION

The principle problem of CAD in CTC is to detect protruding structures (polyps, haustral folds, et.) on the extremely flexible colon wall and to identify the polyps among them. All of the present approaches are based on characterizing the colon wall or the CTC data around the colon wall. The proposed HDF method attempts to enhance the structures of interest and performs the detection and identification tasks as part of this enhancement. It is, to the best of our knowledge, the first CTC CAD method that employs such a scheme. The idea can also be imporved via PDE-based image processing techniques. This is left for the future research.

REFERENCES

[1] C.G. Coin and F.C. Wollett and J.T. Coin and M. Rowland and R.K. Deramos and R. Dandrea, "Computerized radiology of the colon: A potential screening technique," *Comput. Radiol.*, vol. 7(4), pp. 215–221, 1983.

[2] D.S. Paik and C.F. Beaulieu and R.B. Jeffrey and C.A. Karadi and S. Napel, "Visualization modes for CT colonography using cylindrical and planar map projections" *J. Comput. Assist. Tomogr.*, vol. 24(2), pp. 179–188, 2000.

[3] T.Y. Lee and P.H. Lin and C.H. Lin and Y.N. Sun and X.Z. Lin, "Interactive 3-D virtual colonoscopy system," *IEEE Trans. Inf. Tech. Biomed.*, vol. 3(2), pp. 139–150, 1999.

[4] C.F. Beaulieu and R.B. Jeffrey, Jr. and C. Karadi and D.S. Paik and S. Napel, "Display modes for CT colonography, Part II. Blinded comparison of axial CT and virtual endoscopic and panoramic endoscopic volume-rendered studies," *Radiology*, vol. 212(1), pp. 203–212, 1999.

[5] G. Wang and E.G. McFarland and B.P. Brown and M.W. Vannier, "GI tract unraveling with curved cross sections," *IEEE Trans. Med. Imaging*, vol. 17(2), pp. 318–322, 1998.

[6] D. J. Vining and Y. Ge and D. K. Ahn and D. R. Stelts, "Virtual colonoscopy with computer-assisted polyp detection", *Computer-Aided Diagnosis in Medical Imaging*. Address: Amsterdam, Netherlands: Elsevier Science B.V., pp. 445-452 1999 .

[7] R.M. Summers and C.F. Beaulieu and L.M. Pusanik and J.D. Malley and R.B. Jeffrey, Jr. and D.I. Glazer and S. Napel, "Automated polyp detector for CT colonography: Feasibility study," *Radiology*, vol. 216, pp. 284–290, 2000.

[8] R.M. Summers and C.D. Johnson and L.M. Pusanik and J.D. Malley and A.M. Youssef and J.E. Reed, "Automated polyp detection at CT colonography: Feasibility assessment in a human population," *Radiology*, vol. 219, pp. 51–59, 2001.

[9] G. Kiss and J. Van Cleynenbreugel and M. Thomeer and P. Suetens and G. Marchal, "Computer-aided diagnosis in virtual colonography via combination of surface normal and sphere fitting methods," *European Radiology*, vol. 12, pp. 77–81, 2002.

[10] H. Yoshida and J. Nappi, "Three-dimensional computer-aided diagnosis scheme for detection of colonic polyps," *IEEE Transactions on Medical Imaging*, vol. 20, pp. 1261–1274, 2001.

[11] D. S. Paik and C. F. Beaulieu and G. D. Rubin and B. Acar and R. B. Jeffrey and J. Yee and Y. Dey and S. Napel, "Surface Normal Overlap: A Computer-Aided Detection Algorithm With Application to Colonic Polyps and Lung Nodules in Helical CT," *IEEE Transactions on Medical Imaging*, vol. 23(6), pp. 661–675, 2004.

[12] S. B. Gokturk and C. Tomasi and B. Acar and C. F. Beaulieu and D. S. Paik and R. B. Jeffrey, Jr. and J. Yee and S. Napel, "A statistical 3-D pattern processing method for computer-aided detection of polyps in CT colonography," *IEEE Transactions on Medical Imaging*, vol. 20, pp. 1251–1260, 2001.

[13] B. Acar and C. F. Beaulieu and S. B. Gokturk and C. Tomasi and D. S. Paik and R. B. Jeffrey, Jr. and J. Yee and S. Napel, "Edge Displacement Field-Based Classification for Improved Detection of Polyps in CT Colonography," *IEEE Transactions on Medical Imaging*, vol. 21, pp. 1461–1467, 2002.

[14] F.P. Incropera and D.P. DeWitt, *Fundamentals of Heat and Mass Transfer*. Address: Wiley, 2001

[15] O. Monga and S. Benayoun, "Using partial derivatives of 3D images to extract typical surface features," *Computer Vision and Image Understanding*, vol. 61(2), pp. 171–189, 1995.

[16] D. Chakraborty and L. Winter, "Free-response methodology: Alternate analysis and a new observer-performance experiment," *Radiology*, vol. 174(3), pp. 878–881, 1990.

[17] J. Nappi and H. Yoshida, "Automated detection of polyps with CT colonography: Evaluation of volumetric features for reduction of false-positive findings," *Academic Radiology*, vol. 9, pp. 386–397, 2002.

[18] B. Acar and C.F. Beaulieu and D.S. Paik and J. Yee and R.B. Jeffrey, Jr. and S. Napel, “3D Differential Descriptors for Computer Aided Diagnosis of Colonic Polyps in CTC,” *Radiology*, vol. 225(P), pp. 405, 2002.